Electronic Supplementary Material (ESI) for Journal of Materials Chemistry A.

Supplementary Information

Intercalated $Co(OH)_2$-derived flower-like hybrids composed of cobalt sulfide nanoparticles partially embedded in nitrogen-doped carbon nanosheets with superior lithium storage

*Jun Wang, Fan Bai, Xu Chen, Yanluo Lu and Wensheng Yang**

State Key Laboratory of Chemical Resource Engineering
Beijing University of Chemical Technology
Beijing 100029 (P.R. China)
*E-mail: yangws@mail.buct.edu.cn

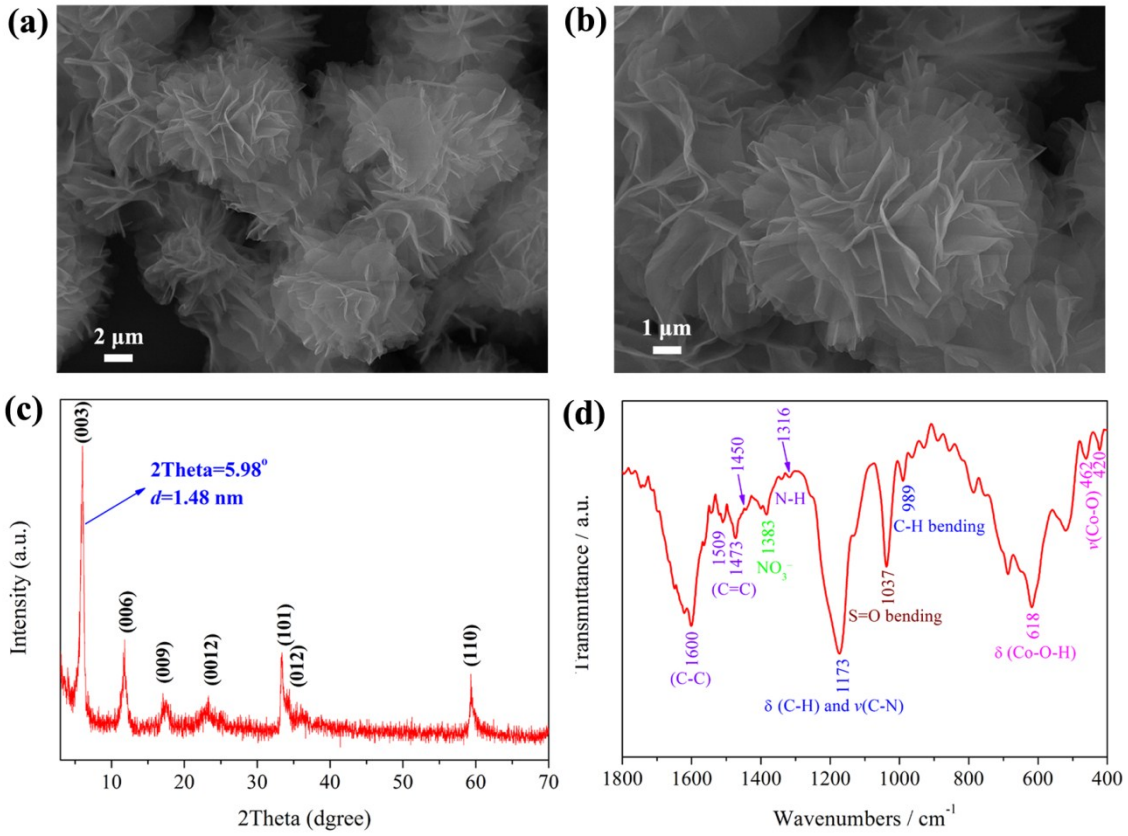

Fig. S1 (a,b) SEM images, (c) XRD pattern and (d) FT-IR spectrum of metanilic-$Co(OH)_2$ precursor.

The SEM images (Fig. S1a and b) show that the metanilic-$Co(OH)_2$ precursor are well-dispersed with size about 4 μm and has a flower-like morphology composed of numerous nanosheets. The XRD pattern (Fig. S1c) shows the characteristic series of basal and higher order (00*l*) reflections at low angles with a layer distance (d_{003}) of 1.48 nm, giving an effective separation of 1.01 nm to accommodate the metanilic anions (assuming a 0.47 nm thickness for the hydroxide layer). The FT-IR spectrum of metanilic-$Co(OH)_2$ precursor (Fig.. S1d) exhibits four strong bands at 1600, 1509, 1473 and 1450 cm^{-1} and a weak band at 1316 cm^{-1}, which are characteristic absorptions of metanilic anions. The bands at 1037 cm^{-1} is characteristic absorptions of the symmetric vibration of S=O. The bands below 620 cm^{-1} are associated with Co-O stretching and Co-OH bending vibrations. These results indicated metanilic anions have been successfully intercalated into the layers of $Co(OH)_2$.

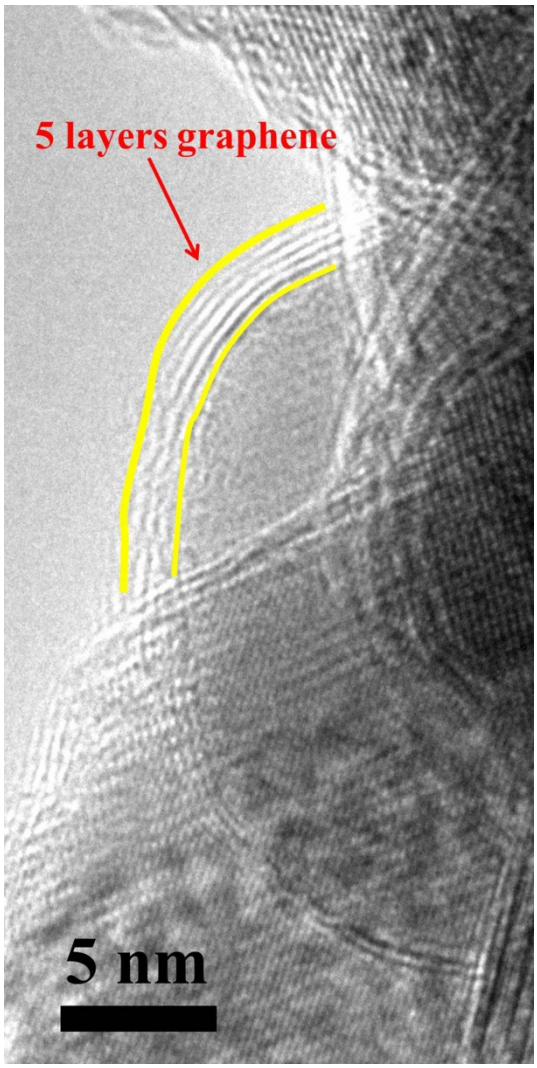

Fig. S2 HRTEM image of a perpendicular nanoflake of $Co_9S_8/Co_{1-x}S$@NC composite.

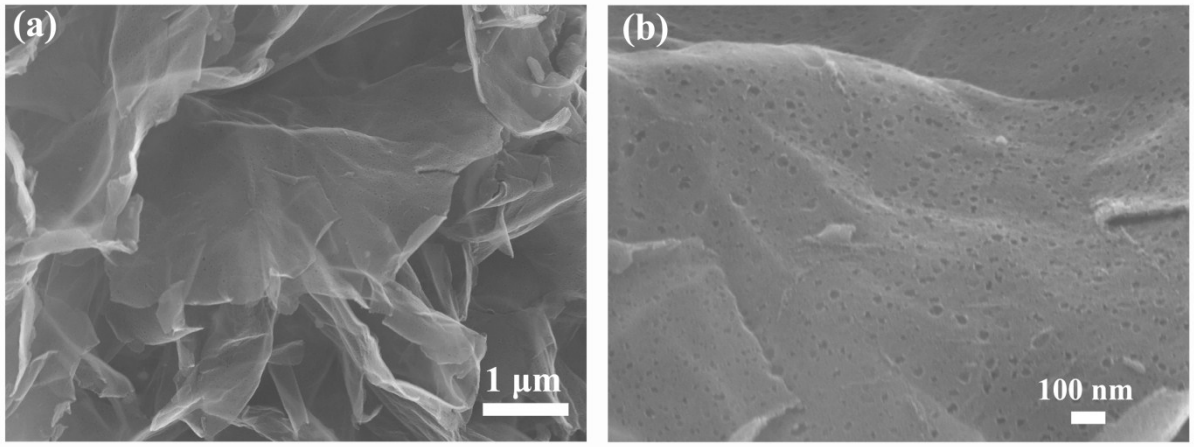

Fig. S3 (a,b) SEM images of $Co_9S_8/Co_{1-x}S$@NC composite after remove the cobalt sulfide nanoparticles.

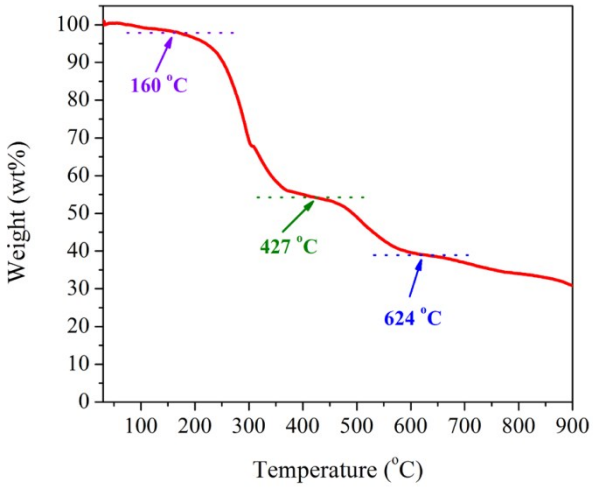

Fig. S4 TG curve of the mixture of metanilic-$Co(OH)_2$ precursor and S powders with a mass ratio of 1:0.75.

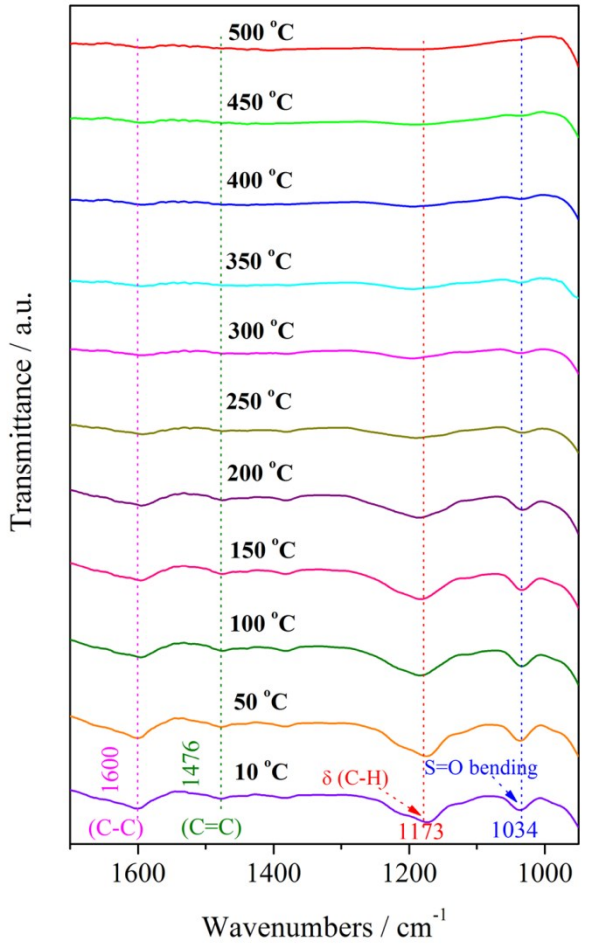

Fig. S5 *In situ* FT-IR spectra of the mixture of metanilic-$Co(OH)_2$ precursor and S powders with a mass ratio of 1:0.75 from 10 °C to 500 °C.

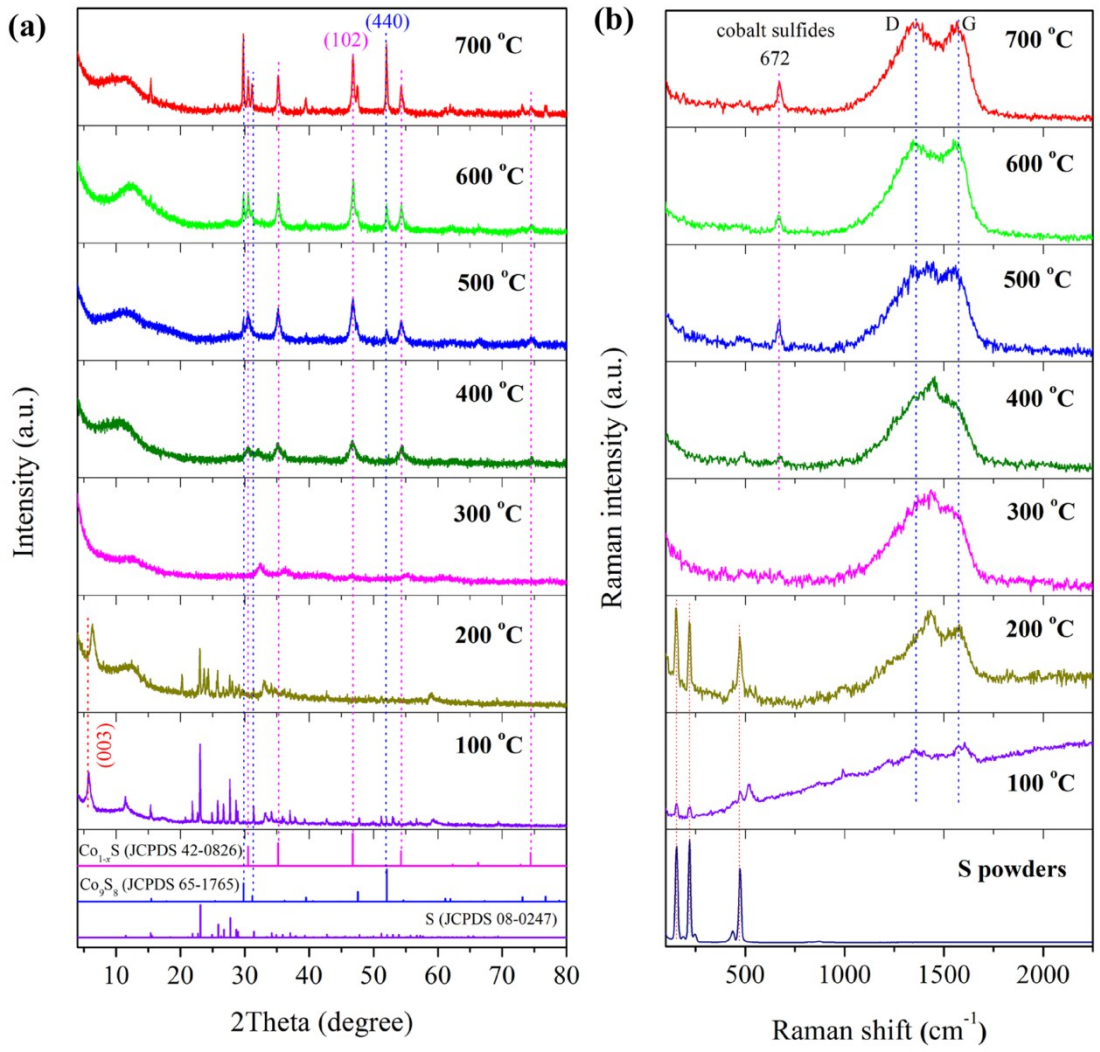

Fig. S6 (a) XRD patterns of the products obtained by pyrolyzing the mixture of metanilic-$Co(OH)_2$ precursor and S powders with a mass ratio of 1:0.75 at various temperatures (100−700 °C). (b) Raman spectra of the products obtained by pyrolyzing the mixture of metanilic-$Co(OH)_2$ precursor and S powders with a mass ratio of 1:0.75 at various temperatures (100−700 °C) and the S powders.

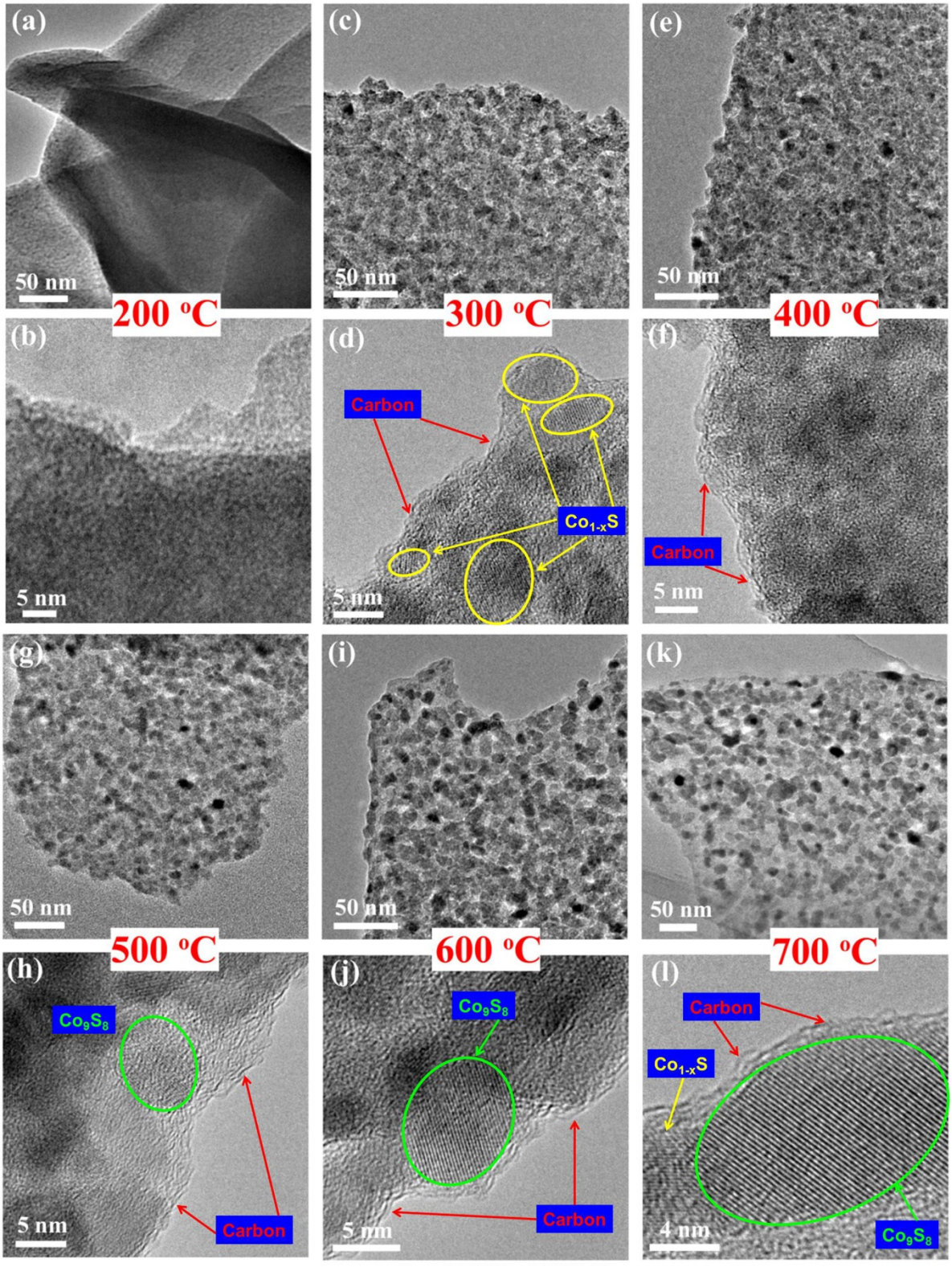

Fig. S7 HRTEM images of the products obtained by pyrolyzing the mixture of metanilic-$Co(OH)_2$ precursor and S powders with a mass ratio of 1:0.75 at various temperatures: (a, b) 200 °C, (c, d) 300 °C, (e, f) 400 °C, (g, h) 500 °C, (i, j) 600 °C and (k, l) 700 °C.

To investigate the mechanism of the carbonization process of metanilic anions within the layers of $Co(OH)_2$, the TG (Fig. S4) and *in situ* FT-IR (Fig. S5) measurements for the mixture of metanilic-$Co(OH)_2$ precursor and S powders with a mass ratio of 1:0.75 were conducted under nitrogen atmosphere. Moreover, XRD (Fig. S6a), Raman (Fig. S6b) and HRTEM (Fig. S7) measurements for the products obtained by pyrolyzing the mixture of metanilic-$Co(OH)_2$ precursor and S powders with a mass ratio of 1:0.75 at various temperatures (100−700 ^oC) were also performed.

The TG curve indicates four general steps of weight loss. The first step, corresponding to the removal of physisorbed water, occurs from room temperature to about 160 ^oC (*Adv. Mater.*, 2013, 25, 1124; *Eur. J. Inorg. Chem.*, 2006, 17, 3442). In this process, the metanilic anions are stable and not decomposed, which is confirmed by the FT-IR spectra due to the four characteristic bands of metanilic anions have not a significant change. The S powders keep solid state and are not sublimated due to the S peaks still can be clearly observed in the XRD patterns and the Raman spectra. The layered structure of $Co(OH)_2$ is still preserved due to the (003) peak in the XRD pattern still can be observed at 200 ^oC.

The second step is observed from 160 to 427 ^oC. During this process, the decomposition and carbonization of metanilic anions occurs from 200 to 400 ^oC to form the cabon nanosheets, which is confirmed by the FT-IR spectra, due to the four characteristic bands of metanilic anions weaken remarkably from 200 ^oC and almost disappear when the temperature above 400 °C. The sublimation of S occurs from 200 to 300 ^oC, because the S peaks cannot be observed in the XRD pattern and the Raman spectrum at 300 °C. The decomposition of $Co(OH)_2$ layers and initial formation of $Co_{1-x}S$ phase occurs at about 300 ^oC due to the (003) peak metanilic-$Co(OH)_2$disappears in the XRD pattern and the $Co_{1-x}S$ phase is observed in the HRTEM images of the product calcined at 300 ^oC. When the temperature increases to 400 ^oC, the diffraction peaks indexed to $Co_{1-x}S$ phase in the XRD pattern and the weak peak at 672 cm^{-1} assigned to cobalt sulfides in the Raman spectrum further confirm the $Co(OH)_2$ layers have been decomposed and converted to $Co_{1-x}S$. Therefore, the second process involves the decomposition and carbonization of metanilic anions to form the carbon nanosheets, the sublimation of S, the decomposition of $Co(OH)_2$ layers and the simultaneous formation of $Co_{1-x}S$. Due to the decomposition and carbonization of metanilic anions is accompany by the the formation of $Co_{1-x}S$, the $Co_{1-x}S$ nanoparticles can be embedded within the carbon nanosheets.

The third process is observed from about 427 to 624 ^oC. In this process, part $Co_{1-x}S$ is gradually converted to Co_9S_8 due to the weak XRD peaks indexed to Co_9S_8 phase can be observed at 500 ^oC and

the peak intensity ratio of $I_{(440)}$ (from Co_9S_8) to $I_{(102)}$ (from $Co_{1-x}S$) increases with increasing temperature. Meanwhile, the peak width of Co_9S_8 and $Co_{1-x}S$ phase in the XRD spectra decreases with increasing temperature, indicating the crystallinity of Co_9S_8 and $Co_{1-x}S$ increases, which also can be confirmed by the HRTEM images. The Raman spectra show the D band and G band are more separable with increasing temperature, indicating the graphitization degree increases with increasing temperature although the graphitized degree of carbon nanosheets still is low. Therefore, this process includes the transformation of part $Co_{1-x}S$ to Co_9S_8 and the further carbonization of the carbon nanosheets to improve the graphitized degree.

The fourth step is above 624 °C, the XRD pattern indicates the further transformation of $Co_{1-x}S$ to Co_9S_8, and the Raman spectrum and the HRTEM images indicate the further improvement of graphitized degree. Therefore, this process involves the further transformation of $Co_{1-x}S$ to Co_9S_8 phase and the further improvement of graphitized degree of the carbon nanosheets.

As a conclusion, the decomposition and carbonization of metanilic anions occurs from 200 to 400 °C to from the carbon nanosheets, which is accompany by the sublimation of S, the decomposition of $Co(OH)_2$ layers and the simultaneous formation of $Co_{1-x}S$, therefore, the $Co_{1-x}S$ nanoparticles can be embedded within the carbon nanosheets. With increasing of the temperature, part $Co_{1-x}S$ is gradually converted to Co_9S_8 and the graphitized degree of the carbon nanosheets is further improved.

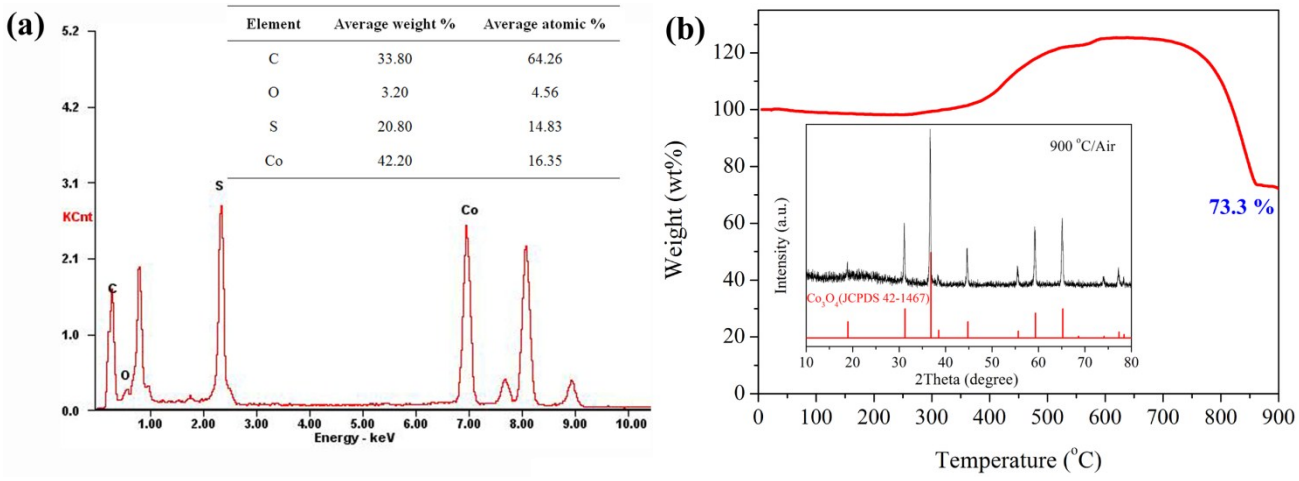

Fig. S8 (a) EDS spectrum and (b) TG curve of $Co_9S_8/Co_{1-x}S$@NC composite; the inset in (b) is the XRD pattern of $Co_9S_8/Co_{1-x}S$@NC composite after the calcination in air at 900 ^oC.

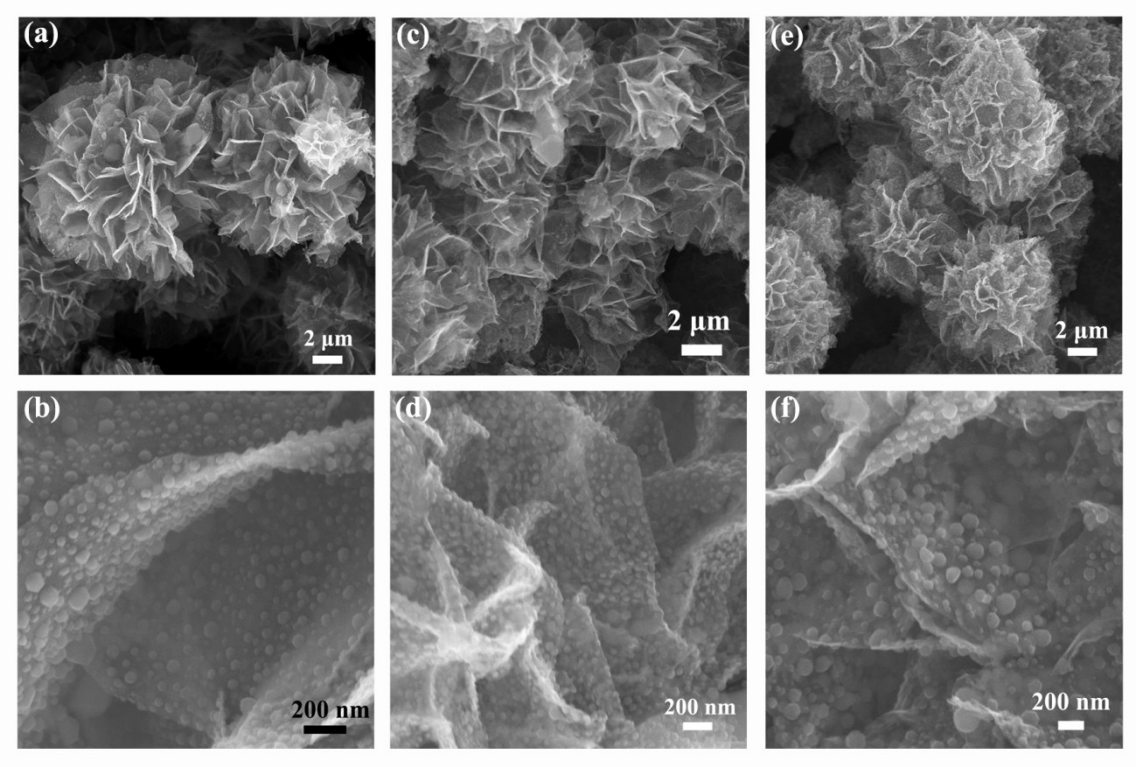

Fig. S9 SEM images: (a, b) $Co_9S_8/Co_{1-x}S$@NC-0.25, (c, d) $Co_9S_8/Co_{1-x}S$@NC-0.50, and (e, f) $Co_9S_8/Co_{1-x}S$@NC-1.0 composites.

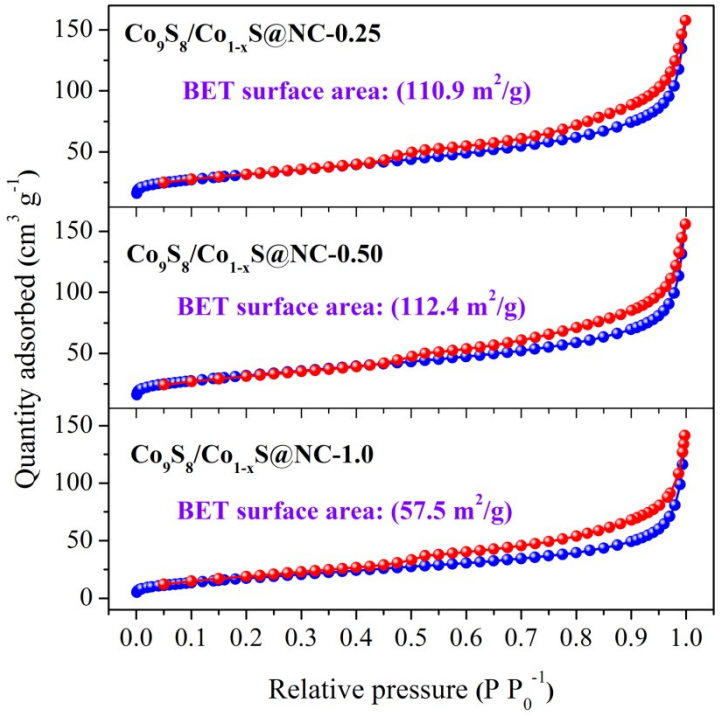

Fig. S10 Nitrogen adsorption/desorption isotherms of $Co_9S_8/Co_{1-x}S$@NC-*x* composites (where *x* is 0.25, 0.50, and 1.0).

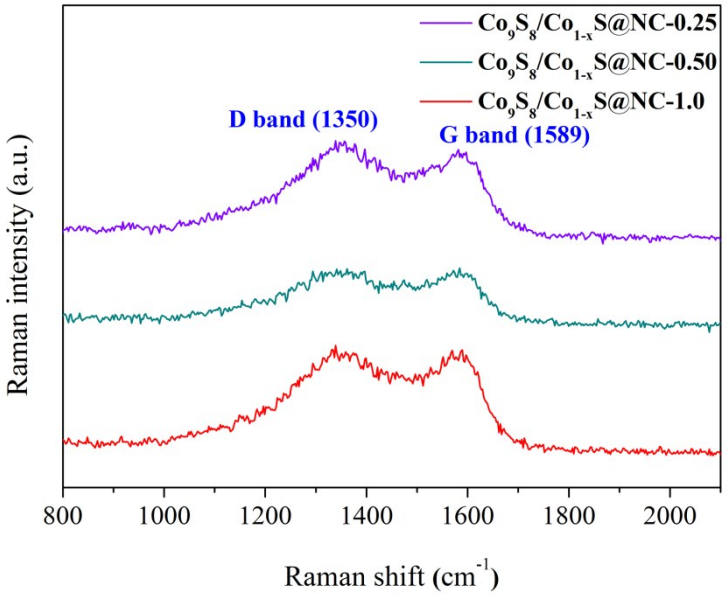

Fig. S11 (a) Raman spectra of $Co_9S_8/Co_{1-x}S$@NC-*x* composites (where *x* is 0.25, 0.50, and 1.0).

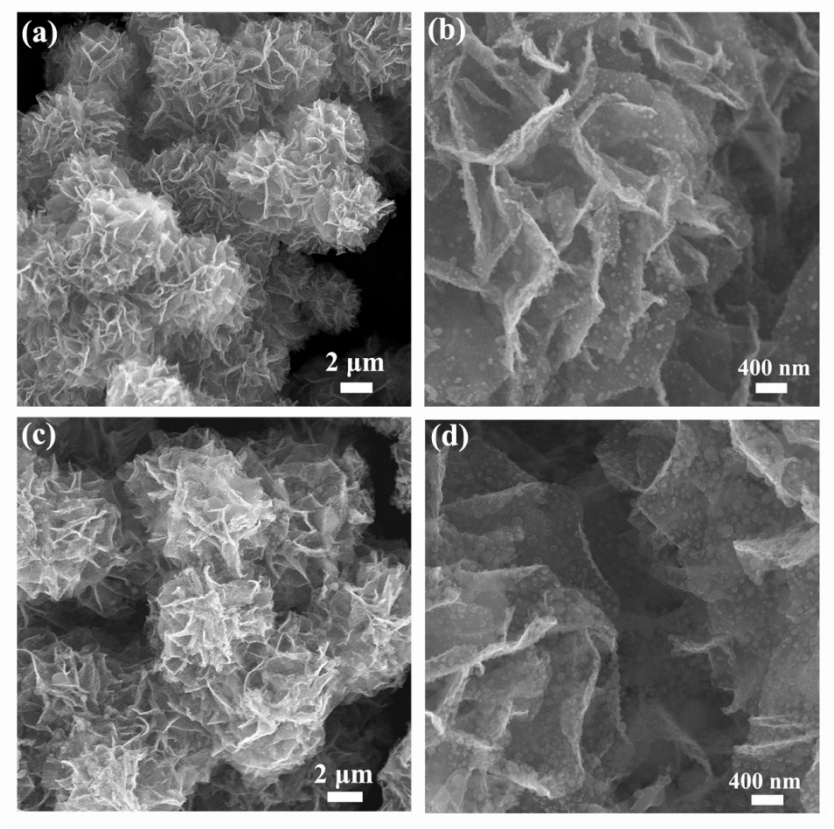

Fig. S12 SEM images of $Co_9S_8/Co_{1-x}S$@NC composite obtained at (a, b) 800 °C, and (c, d) 1000 °C.

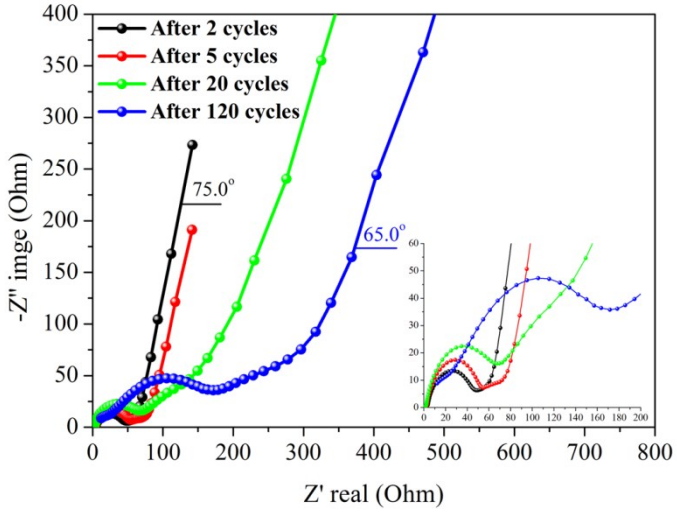

Fig. S13 Nyquist plots of $Co_9S_8/Co_{1-x}S$@NC-0.75 electrode (obtained at 900 °C) at 0.1 V after 2, 5, 20 and 120 cycles.

Table S1. The C, N, S, and H contents derived from elemental analysis.

Sample	C (wt%)	N (wt%)	S (wt%)	H (wt%)
$Co_9S_8/Co_{1-x}S$@NC-0.25	13.16	0.60	22.96	0.81
$Co_9S_8/Co_{1-x}S$@NC-0.50	12.32	0.74	29.51	0.70
$Co_9S_8/Co_{1-x}S$@NC-0.75	13.43	0.69	30.05	0.89
$Co_9S_8/Co_{1-x}S$@NC-1.0	13.62	0.85	30.42	0.68

Table S2. Performance comparison of $Co_9S_8/Co_{1-x}S$@NC-0.75 in this work and the cobalt sulfides-based electrodes reported in literatures.

Materials	Reversible capacity ($mAh\ g^{-1}$)	Rate performance ($mAh\ g^{-1}$)	Capacity retention (cycling range) ($mAh\ g^{-1}$)	Ref.
$Co_9S_8/Co_{1-x}S$@NC-0.75	1250 at 50 mA g^{-1}	813 at 2 A g^{-1}	1230 (98.4%), (2–110 cycles)	This work
MWCNT@a-C@Co_9S_8	805 at 1 A g^{-1}	646 at 2 A g^{-1}	662 (82.2%), (6–120 cycles)	[6]
rGO/$Co_9S_8/Co_{1-x}S$	748 at 200 mA g^{-1}	547 at 2 A g^{-1}	994 (132.9%), (2–150 cycles)	[8]
Co_9S_8/graphitic carbon	1770 at 100 mA g^{-1}	692 at 3 A g^{-1}	1600 (90.4%), (2–40 cycles)	[11]
C@Co_9S_8 dandelion	636 at 1 A g^{-1}	373 at 6 A g^{-1}	520 (81.8%), (2–50 cycles)	[17]
RGO/Co_9S_8	595 at 545 mA g^{-1}	534 at 1.1 A g^{-1}	382 (64.2%), (2–500 cycles)	[19]
Co_9S_8@C fibers	1105 at 54 mA g^{-1}	318 at 2.7 A g^{-1}	872 (78.9%), (2–100 cycles)	[23]
Co_9S_8-coated carbon	637 at 100 mA g^{-1}	351 at 1 A g^{-1}	540 (84.8%), (2–300 cycles)	[24]
Co_9S_8-650	1040 at 100 mA g^{-1}	635 at 2 A g^{-1}	1400 (134.6%), (2–100 cycles)	[13]
Flower-like $Co_{1-x}S$	928 at 100 mA g^{-1}	—	485 (52.6%), (2–150 cycles)	[44]
CoS_2/RGO	1499 at 100 mA g^{-1}	440 at 2 A g^{-1}	1245 (83.1%), (2–150 cycles)	[5]
CoS_2 polyhedron	738 at 100 mA g^{-1}	155 at 1 A g^{-1}	694 (94.0%), (2–100 cycles)	[10]
CoS_2/fCNT	691 at 200 mA g^{-1}	338 at 1 A g^{-1}	900 (130.2%), (2–180 cycles)	[14]
NC/CoS_2-650	700 at 100 mA g^{-1}	340 at 2.5 A g^{-1}	560 (80%), (2–50 cycles)	[15]
CoS_2/graphene	805 at 50 mA g^{-1}	360 at 0.8 A g^{-1}	630 (78.3%), (2–40 cycles)	[18]
CoS_2/graphene	890 at 100 mA g^{-1}	641 at 1 A g^{-1}	800 (89.9%), (2–150 cycles)	[20]
CoS_2 Hollow sphere	925 at 50 mA g^{-1}	—	320 (34.6%), (2–40 cycles)	[43]
CoS_2 hollow prisms	867 at 1 A g^{-1}	470 at 5 A g^{-1}	737 (85.0%), (2–200 cycles)	[47]
worm-like CoS_2	1140 at 100 mA g^{-1}	501 at 2 A g^{-1}	883 (77.5%), (2–100 cycles)	[48]
CoS@PCP/CNTs-600	1278 at 200 mA g^{-1}	752 at 10 A g^{-1}	1668 (130.5%), (2–100 cycles)	[9]
N-doped carbon@CoS	750 at 2A g^{-1}	641 at 4 A g^{-1}	671 (89.5%), (2–1400 cycles)	[22]
CoS/Ni core-branch	672 at 1C	371 at 6C	670 (99.7%), (2–200 cycles)	[45]
CoS/graphene	1200 at 59 mA g^{-1}	391 at 1.77 A g^{-1}	898 (74.8%), (2–80 cycles)	[46]
Cobalt sulfides/GNS	1018 at 100 mA g^{-1}	680 at 1 A g^{-1}	954 (93.7%), (2–50 cycles)	[21]
$NiCo_2S_4$ nanotube	1180 at 140 mA g^{-1}	212 at 2.8 A g^{-1}	710 (60.2%), (2–50 cycles)	[49]